

Validation of the Doppler Shifted Dispersion Relation for Waves in the Presence of Strong Tidal Currents, using ADCP Wave Directional Spectra and Comparison Data.

B. Strong and B. Brumley
RD Instruments
9855 Business Park Ave.
San Diego, CA, USA 92131
Bstrong@rdinstruments.com

E.A. Terray
Department of Applied Ocean Physics and Engineering
Woods Hole Oceanographic Institution
Woods Hole, MA, USA 02543

N. C. Kraus
U.S. Army Corps of Engineers
CEERD – HC, 3909 Halls Ferry Rd.
Vicksburg, MS, USA 39180

1. Introduction

Waves propagating through regions of strongly varying mean flows, such as occur at the edges of ocean boundary currents, or the mouths of harbors and estuaries, are modified substantially by their interaction with the flow (this is nicely illustrated by Figure 1, which shows ADCP observations taken off the southern coast of England near Eastbourne, Sussex). The sea states that result, particularly in the case of adverse waves and currents, can be a hazard to mariners, present challenges in the design of coastal structures, and are active transporters of sediment in the nearshore region. Wave-current interaction has been investigated in the laboratory (Thomas, 1981), and several authors (Battjes, 1982; Gonzalez, 1984) have studied it in the field (interestingly, neither of the latter studies included direct measurements of near-surface currents, relying instead on tidal models to provide this information). Although originally developed for current measurement, upward-looking acoustic Doppler current profilers (ADCPs) have proven also to be useful for sensing waves. Recent work has demonstrated that they are capable of measuring the frequency-directional distribution of surface waves with a fidelity equivalent, and in many cases superior, to those obtained from bottom-mounted PUV wave gages (Strong *et al.*, 2000; Terray *et al.*, 1999, 1997, 1990; Gordon *et al.*, 1998; Hashimoto, 1997). A unique strength of this approach is that a single compact instrument yields simultaneous information about the waves in conjunction with full water column profiles of the current.

In this contribution we show that both kinematic and dynamic aspects of the modulation of waves by currents can be seen in measurements obtained from an ADCP “Wave Gage”. Our purpose is to illustrate, by means of a few examples, the utility of this sensor for addressing questions related to wave-current interaction. We conclude the paper

with a slightly different application, in which we use time series of measured wave height spectra to estimate the direction, range and duration of distant storm events.

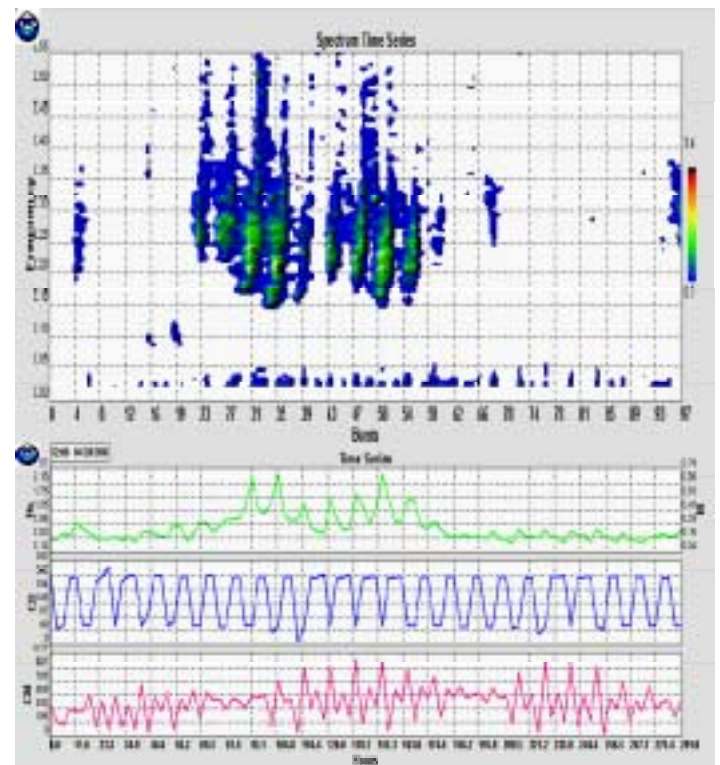


Figure 1. ADCP data showing the modulation of wave amplitude by tidal currents. Top panel: spectrogram of wave height (time is in 4 hr. “bursts”). Bottom panel: time series of significant height H_s (ft), current direction CD (degT), and current magnitude CM (mm/s). The water depth was 5m.

2. Kinematics of Waves on Currents

The dispersion relation for waves travelling on a vertically-sheared current $U(z)$ has been analyzed by Kirby and Chen (1989) for the case of weak currents. Expanding in terms of the small parameter $\epsilon=U/c$, where c is the wave phase speed, they found that through $O(\epsilon)$

$$(\omega - kU \cos \alpha)^2 = gk \tanh(kH) \quad (2.1)$$

where ω and k are the bottom-relative radian frequency and wavenumber (*i.e.* those observed in a fixed reference frame), H is the water depth, and α denotes the included angle between the directions of wave propagation and the current. Note that equation (2.1) is just the usual dispersion relation for arbitrary water depth applied to the frequency observed in a reference frame moving with the current (*i.e.* the *intrinsic* frequency $\omega - \mathbf{k} \cdot \mathbf{U}$). Kirby and Chen show that at this order U should be taken to be the depth average of $U(z)$ over the normalized energy distribution of the waves

$$U = \int_{-H}^0 dz E(\omega, z) U(z) \Big/ \int_{-H}^0 dz E(\omega, z) . \quad (2.2)$$

We remark that the ADCP is particularly useful in this regard because it can measure the current profile over the region in which wave energy is concentrated.

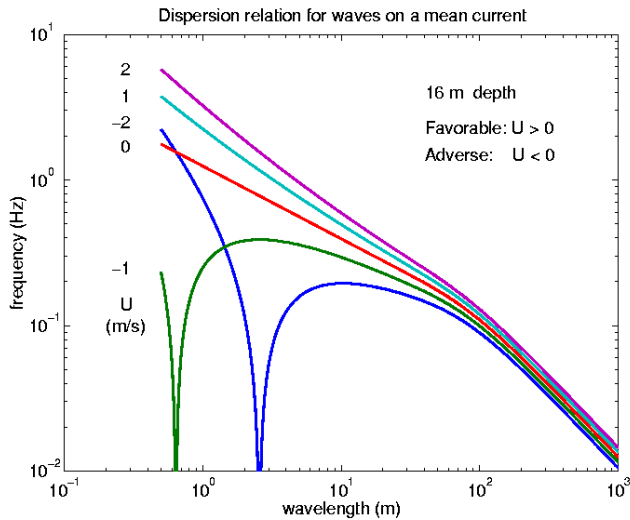


Figure 2. Relation between wavenumber and measured frequency in 16 m water depth for co-linear waves and currents (with and against), and current speeds between ± 2 m/s.

We plot the dispersion relation (2.1) in Figure 2. When the current flows in the same direction as the waves ($U > 0$) there is a unique solution for k at each frequency. For adverse currents ($U < 0$) the frequency $\omega(k)$ vanishes for waves having

a phase speed ω/k equal to the current speed, and has a local maximum for the wave whose group velocity $d\omega/dk$ equals U . For frequencies above this local maximum the solution for the wavenumber $k(\omega)$ is seen to be unique, whereas at lower frequencies there are three solutions. In the latter case we use the smallest wavenumber solution since we are interested in the energy-containing part of the spectrum. The dispersion relation is used in several ways. We estimate the wave directional spectrum by the Iterative Maximum Likelihood Method (Krogstad *et al.*, 1988) which requires a model of the ADCP response, $H(\mathbf{k})$, to a monochromatic wave propagating at an arbitrary angle. Consequently at each frequency we compute $k(\omega, \alpha)$ over all angles from $0-360^\circ$ (typically in 4° increments), and use this to determine the response function H . To calculate the non-directional spectrum of surface displacement from either pressure or orbital velocity we use the wavenumber $k_p(\omega)$ corresponding to the direction α_p of the dominant wave at that frequency. Use of the correct wavenumber is important when computing spectra of surface displacement from subsurface pressure or velocity measurements. For example, in the case of a bottom-mounted pressure gage, the Fourier amplitudes of wave height and pressure are related (via linear theory) by

$$\hat{p}(\omega | z = -H) = \rho g \hat{a}(\omega) \cosh(kH) . \quad (2.3)$$

Hence the amplitude spectrum of wave height, $A(\omega)$, estimated using the true wavenumber, k , and the corresponding quantity $A_0(\omega)$, computed from equation (2.3) using the wavenumber k_0 obtained from (2.1) when the current is neglected, are related by

$$A(\omega)/A_0(\omega) = \cosh(kH)/\cosh(k_0H) . \quad (2.4)$$

In the case of a favorable current ($U > 0$), Figure 2 shows that $k < k_0$, so that $A < A_0$. The situation is reversed for an adverse current ($U < 0$), in which case $A > A_0$.

3. Grays Harbor Data

We illustrate the kinematics and dynamics of waves riding on currents using data collected during two deployments of a bottom-mounted ADCP at Grays Harbor, WA (roughly 46.8°N , 124.2°W – see Figure 3). The first deployment took place from 13 September through 11 October, 1999 near the mouth of the harbor in a nominal water depth of 17m, and included a co-located ADV (PUV-type) wave gage. For the second deployment (15 October - 15 November, 1999) the ADCP was placed on the bottom farther east into the channel at 15 m depth. In both deployments data were collected every four hours in bursts of roughly 34 minutes (4096 points at a 2 Hz sample rate). The maximum current in the first data set was roughly 1 m/s, reaching almost 2m/s during the second deployment.

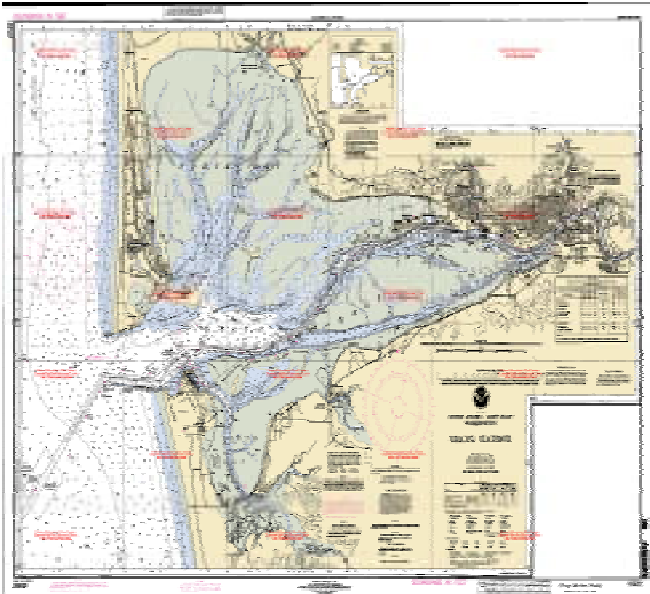


Figure 3. Coastal bathymetry in the vicinity of Grays Harbor, WA. The shore normal is approximately 260°T.

4. Observations of Wave Kinematics

Time series of significant wave height, peak period, peak direction, and tidal excursion during the first deployment are shown in Figure 4. The time series of significant height is seen to be modulated at the tidal period, although the degree of modulation is less than that shown in Figure 1 due to the relatively longer wavelengths of the waves in this case. A similar periodicity is also evident in the spectrogram of wave height shown in Figure 5. A careful examination of that figure shows that the spectrum at higher frequencies is enhanced during outgoing (ebb) and reduced during incoming (flood) tides.

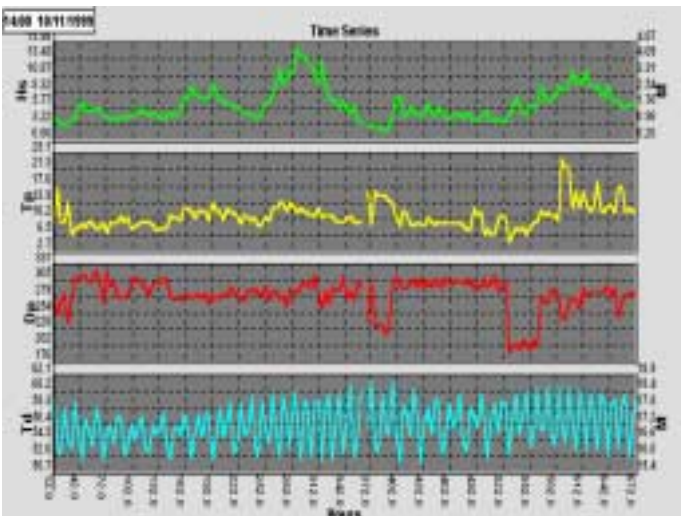


Figure 4. Time-series of significant wave height (H_s , ft), peak period (T_p), peak direction (D_p , degrees), and tidal elevation (T_d , ft) as a function of time (hours). The right-hand scale gives wave height and tidal elevation in meters.

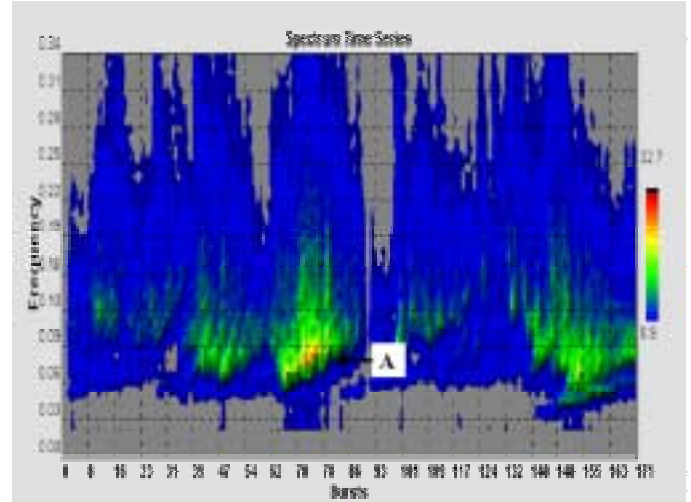


Figure 5. Spectrogram of wave height computed from 34 minute bursts of data taken every 4 hours.

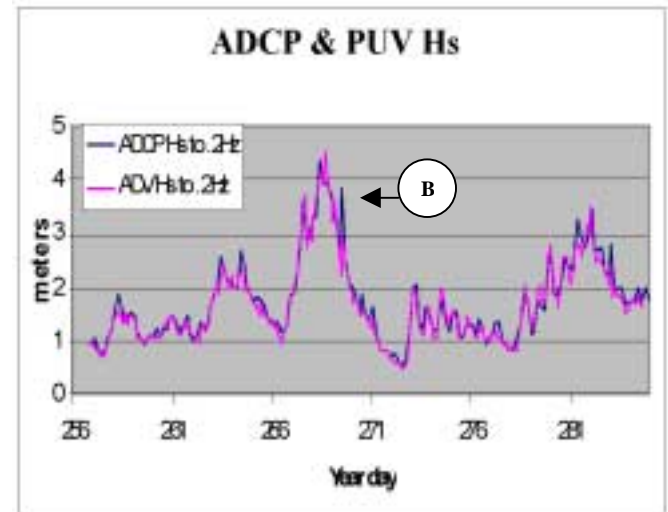


Figure 6. Time-series of significant wave height computed from frequency components below 0.2 Hz. The ADCP estimate was obtained from range cells close to the surface, and wave height was estimated using the correct wavenumber. The presence of a current was not included in the analysis of the ADV-PUV measurements.

The first Grays Harbor deployment included a co-located ADV-PUV directional wave gage. The PUV data were analyzed using software that did not account for the presence of the tidal current. Although the ADCP-derived wave parameters compared well most of the time with those estimated from the PUV gage (Strong, *et al.*, 2000), there were discrepancies during periods of maximal current. This can be seen in Figure 6 which shows the significant wave height for waves with frequencies below 0.2 Hz estimated from both the ADCP and PUV sensors. The difference between these two estimates is shown in Figure 7, where it is seen to correlate strongly with the tidal current.

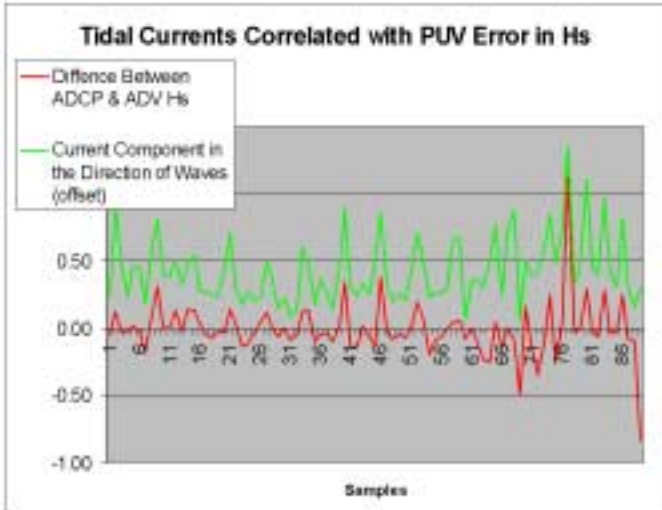


Figure 7. The difference between ADCP and PUV estimates of significant wave height shown in Figure 6. The component of the tidal current in the direction of the waves is also shown (this curve has been shifted upward, and the scale is arbitrary).

We focus on a case where the disagreement between the two sensors is large. This is marked “B” in Figure 6, and occurred at 1400 PDT on 26 September, 1999. Figure 8, below, shows the measured current profile and wave direction for this burst.

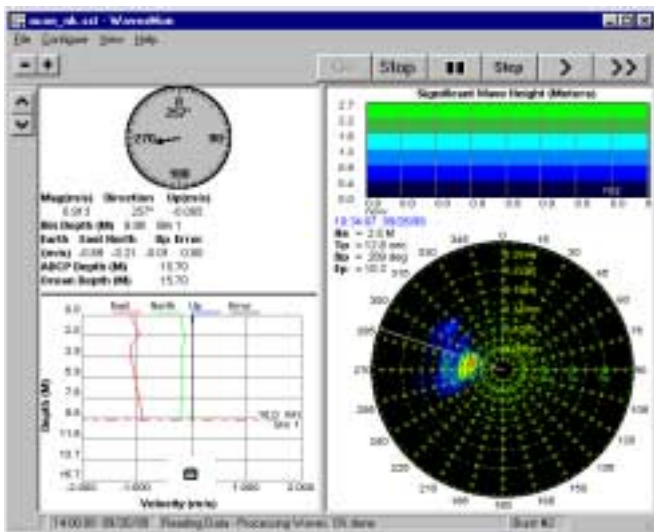


Figure 8. “WavesMon” software display showing ADCP currents and waves for the burst at 1400 (PDT) on 26 September, 1999.

The depth-averaged current is flowing west out of the harbor at roughly 1 m/s. The shear at depths below 3 m is close to linear with a value of roughly $4 \times 10^{-2} \text{ s}^{-1}$. This extrapolates to a near-bed velocity of 0.5 m/s, which is in agreement with the average velocity measured by the co-located PUV gage. Current shear contributes directly to the dispersion relation. For a linear shear, the right hand side of equation (1.1) is multiplied by a factor $[1 - (c - U_s) \nabla U / g]$, where ∇U denotes the

vertical shear, and U_s is the current at the surface (Kirby and Chen, 1989). In our case,

$$|(U_s - C) \nabla U / g| < 5 \times 10^{-2} \ll 1,$$

and therefore the direct effect of shear can be neglected. However, shear has another implication when the only estimate of the current available has been obtained near the bed. As an illustration, using a current speed of 0.5 m/s instead of 1 m/s in the dispersion relation (in 17m water depth) produces wavenumbers in error by 6%, 19% and 46% at frequencies of 0.1, 0.2, and 0.3 Hz, respectively. This example shows that even for the case of modest shears, using a measurement of the current near the bed can introduce significant errors.

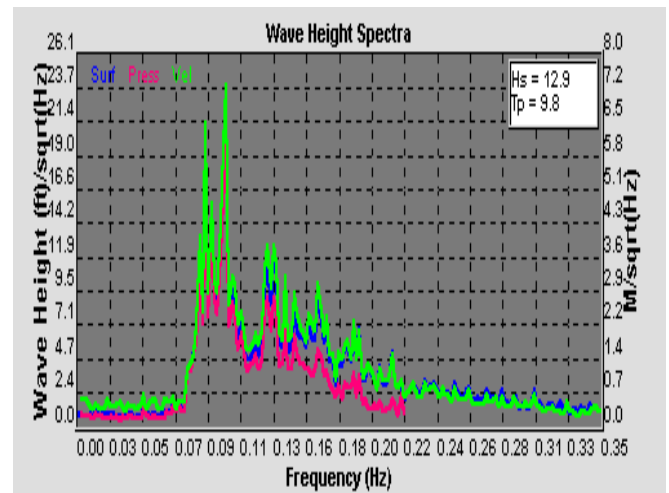


Figure 9. Estimates of the amplitude spectrum ($\text{ft}/\sqrt{\text{Hz}}$) of surface displacement derived from surface echolocation and subsurface orbital velocities (both extend over all frequencies shown), and pressure (to 0.21 Hz) during an adverse (ebb) current of 1 m/s. The presence of a current has been neglected in computing surface spectra from the pressure and velocity measurements.

The ADCP Wave Gage yields three independent estimates of the non-directional wave height spectrum based on pressure, orbital velocity, and echo-location of the surface (“surface-track”). Note that echo-location is a direct measurement of the surface and does not depend on knowing the correct wavenumber.

The wave height spectra derived from these measurements, but neglecting the current, are shown in Figure 9. The pressure measurement (taken at 17m depth) is seen to underestimate the true height spectrum in an adverse current. The magnitude of the discrepancy is a function of frequency, in agreement with our earlier discussion in connection with equation (2.4). For example, in a co-linear adverse current of 1 m/s, 17 m water depth, and for a frequency of 0.18 Hz, we find $k = 0.175 \text{ m}^{-1}$, and $k_0 = 0.133 \text{ m}^{-1}$. Applying equation (2.4) gives $A/A_0 \sim 2$, which is in reasonable agreement with the ratio of echolocation to pressure-derived amplitude

spectra shown in Figure 9. In contrast, at 0.1 Hz, we compute $k = 0.062\text{m}^{-1}$ and $k_o = 0.055\text{m}^{-1}$, so that $A/A_o \sim 1.1$, a value also in agreement with the observations. Although wave height spectra also should be computed from ADCP velocity measurements using the correct wavenumber, in this case the velocity measurements were taken at depths of 1, 2 and 3 m, and hence are relatively insensitive to the effect of the current.

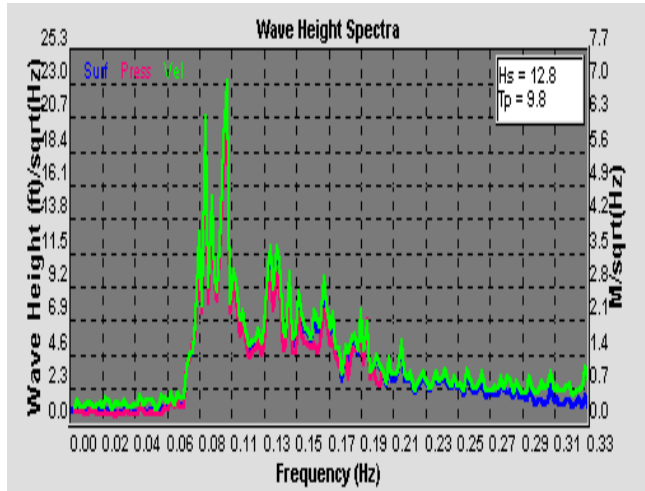


Figure 10. Amplitude spectra as in Figure 8, but the pressure and velocity data now have been converted to surface spectra using the current-dependent wavenumber determined from equation (2.1).

Figure 10 shows the result of using the Doppler corrected wavenumber in the conversion of pressure (and velocity) to wave height at all frequencies. The agreement between the three measurements is excellent, validating equation (2.4).

Table 1. Significant Wave Height on 09/26/99 at 1400 PDT

ADCP Corrected for Currents with 0.35 Hz. cut-off	3.95 m
ADCP Corrected for Currents with 0.22 Hz. cut-off	3.87 m
ADCP Not Corrected for Currents with 0.22 Hz. Cut-off, Using Pressure	2.87 m
ADV Not Corrected for Currents with 0.22 Hz. Cut-off, Using Pressure	2.94 m
Buoy (not co-located)	2.46 m

Although the Doppler correction of the wavenumber mainly affects the higher frequencies in the spectra, its integrated effect on the estimation of significant wave height is not negligible. This is illustrated in Table 1, from which we conclude that when the current is strong, neglecting it can introduce a significant error into the estimate of H_s derived from pressure measurements at the bed.

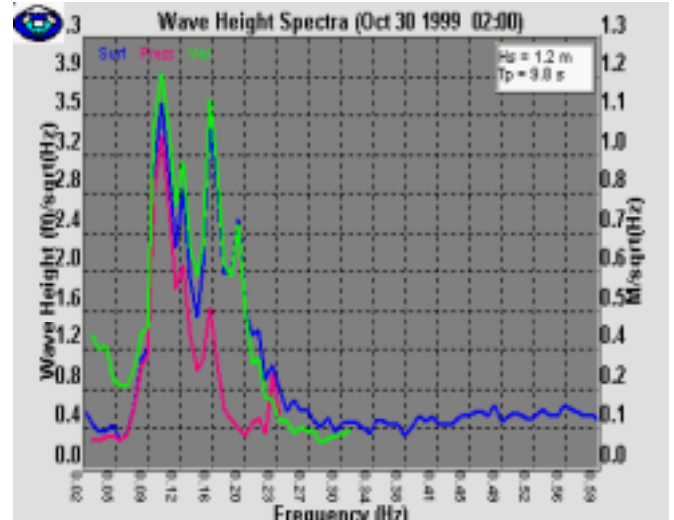


Figure 11. Estimates of the amplitude spectrum ($\text{ft}/\sqrt{\text{Hz}}$) of surface displacement derived from surface echolocation (all frequencies), subsurface orbital velocities (to 0.25 Hz), and pressure (to 0.2 Hz) during an adverse (outflow) current of 1.7 m/s.

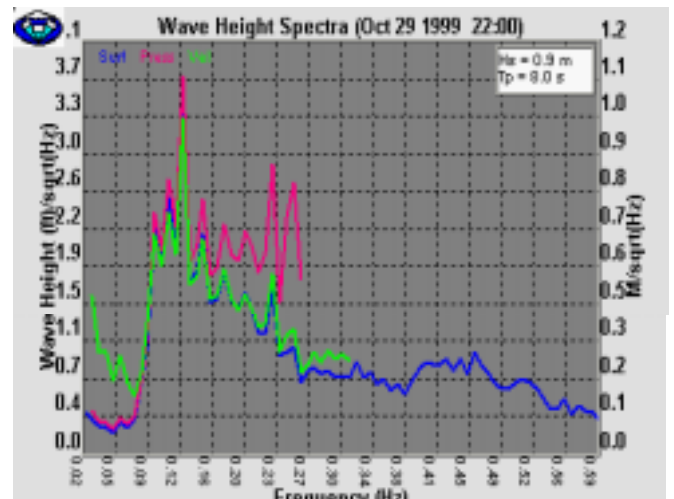


Figure 12. As in Figure 11, but estimated during a favorable (inflow) current of 0.9 m/s.

Figures 11 and 12 show another example of wave height amplitude spectra derived from the pressure, velocity and surface-track by neglecting the effect of the current on the wavenumber. The pressure-derived height is seen to underestimate the true spectrum when the waves and currents are adverse, and to overestimate it when the current is flowing in the same direction as the waves. This behavior is in accord with our conclusions following equation (2.4).

5. Dynamics of Waves on Currents

So far we have only considered kinematic effects, such as the change in wavelength. To determine amplitude changes requires consideration of the dynamics. This problem has been addressed using field observations by Battjes (1982) and Gonzalez (1984). We follow the latter reference here. Energy does not provide the required relation, since the energy of waves propagating through an inhomogeneous current is not conserved due to the rate of working on the current by the wave (“radiation”) stresses. However, if the variation of the current is slow compared to the scale of the waves (*i.e.* the system is only weakly nonlinear) a related quantity, the wave action $\Lambda = E/\sigma$, is conserved (here E denotes the wave energy density computed from linear theory, and $\sigma = \omega - \mathbf{k} \cdot \mathbf{U}$ is the intrinsic frequency). We write this as

$$\frac{\partial \Lambda}{\partial t} + \nabla \cdot [(\mathbf{U} + \mathbf{c}_g) \Lambda] = 0 \quad (5.1)$$

where \mathbf{c}_g is the group velocity $d\sigma/d\mathbf{k}$. Then $\mathbf{U} + \mathbf{c}_g$ is the propagation velocity of energy or action in a fixed reference frame (*i.e.* relative to the bottom). The time scale, T , for temporal changes in action density is roughly a tidal period. Hence $\partial \Lambda / \partial t$ can be neglected relative to the flux divergence if the spatial scale of the current, L , is much less than $c_g T \sim O(200)$ km. We assume that this condition is satisfied, and neglect the time dependent term. Making the further assumption that the flux balance is approximately one-dimensional, we find that the local (E) and offshore (E_o), energy densities are related by

$$\frac{E}{E_o} = \frac{U_o + c_{g0} \cos \vartheta_o}{U + c_g \cos \vartheta} \frac{\sigma}{\sigma_o} \quad (5.2)$$

where ϑ and ϑ_o are the angles, respectively, between the wave propagation directions and the shore normal at the local and offshore locations which, by definition in this case, coincides with the direction of the current (Gonzalez, 1984). These angles are related by refraction due either to the bathymetry or the current.

Since we do not have simultaneous measurements of the unperturbed waves (in the absence of currents), it is not possible to use our data to make a direct test of equation (5.2). Instead we use the latter relation to estimate what the offshore wave energy must have been in a region with negligible current ($U_o = 0$, $\sigma_o = \omega$, and $c_{g0} = \omega/2k_o$). Assuming the action is conserved, and the system one-dimensional, we expect the offshore energy E_o to be independent of the local current. The result of this exercise, applied to a narrow band of waves centered at 0.3 Hz, is shown in Figure 13.

Note that changes in wave amplitude due to bottom refraction, while contained in the general equation (5.1), are not important for waves of this frequency since, even at the location of the ADCP, they are not depth limited. It is evident that whereas the local energy exhibits a tidal modulation, much of this signature has been removed from the estimate of the offshore energy. The residual modulation can be due to several factors not accounted for in our simple calculation. First, we used the component of the current in the direction of the dominant wave, rather than the mean direction of the waves in the frequency band around 0.3 Hz. This appears to be a reasonable approximation for many of the spectra, but has not been checked thoroughly. Second, equation (5.2) is based on a one-dimensional model, and neglects lateral current variation (see Battjes, 1982, for a discussion). Third, we do not include wind forcing of either the waves or currents (for action to be conserved, the combined wave-current system be stationary). Fourth, there might be a non-negligible offshore tidal current that is coherent with the flow at our measurement site. Fifth, although bottom-refraction for waves in this band is not important, $U/c \sim 0.2$, so that refraction by the current might be important. Lastly, we used the mean current rather than using the vertical-weighting given by equation (2.2). The sensitivity of our result to these factors has not been explored. However, the simple analysis here removes much of the tidal modulation, suggesting that the effects listed above amount to a relatively small correction.

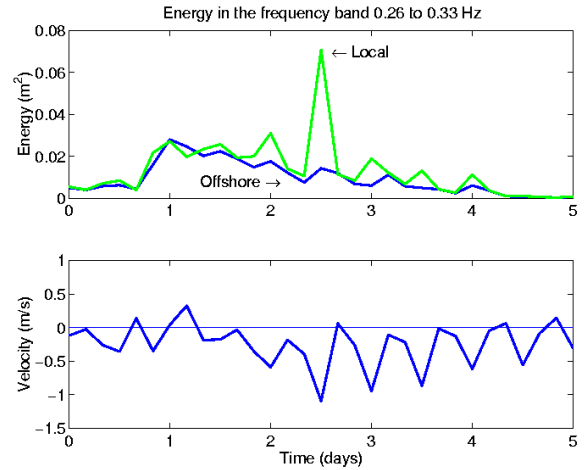


Figure 13. Top panel: Offshore energy E_o (*i.e.* in deep water with negligible current) of waves in the frequency band 0.26-0.33 Hz deduced from the locally-measured energy E using equation (5.2). Note that offshore energy was calculated and then band-averaged. Bottom panel: Component of the local current in the dominant wave direction. $U < 0$ represents an adverse (outgoing) current.

6. Refraction Due to Bathymetry

“Point” wave direction sensors, such as PUV triplets and directional buoys (either 3-D acceleration, or pitch-roll-heave) yield estimates of the first three (complex) coefficients in the Fourier expansion of the directional distribution, and hence these sensors cannot resolve multidirectional spectra without additional modeling assumptions.

In contrast, the ADCP measures wave velocities at a number of horizontal positions (and depths) within the wave field. The collection of these measurement volumes constitutes a compact spatial array from which the directional distribution of the waves can be estimated by applying the Iterative Maximum Likelihood Method (Krogstad *et al.*, 1988) to “invert” the forward model for the expected array cross-spectra. As a result, for the frequencies encountered here, the ADCP wave gage produces relatively high directional resolution (this, of course, is also a function of the analysis technique), and as a result resolve multimodal directional distributions (within a given frequency band).

The utility of the ADCP for studying wave refraction is illustrated by Figure 14, which shows the average directional distribution of the waves over the period 2-5 October, 1999. An energetic band of waves (at frequencies above 0.1 Hz) arriving from the northwest (~305°T) is evident, as well as a second weaker system from a more southerly direction (~210°T). The very longest waves have been turned to propagate in the shore-normal direction (~260-265°T).

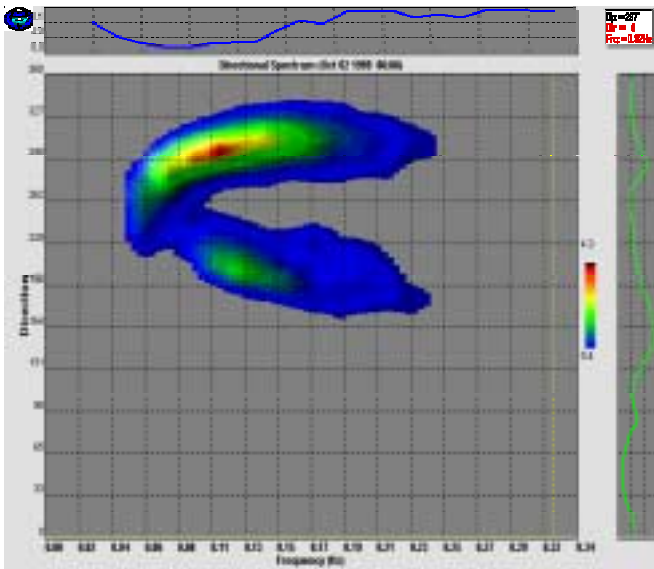


Figure 14. Average ADCP directional spectrum from Grays Harbor in 17m water depth for the period 2-5 October, 1999. The shore normal is approximately 260-265°T.

Although properly speaking, to model this result one should integrate the ray equations from deep water to the nearshore measurement site, in practice the shelf is relatively narrow

and consequently Snell’s law provides a reasonable first order approximation. We assume that the local depth contours are straight. Then the component of the wavenumber along the contours is constant, and therefore

$$k \sin \vartheta = k_0 \sin \vartheta_0 \quad (6.1)$$

where (k_0, ϑ_0) and (k, ϑ) are respectively the offshore and local wavenumber and propagation directions (relative to the shore normal). We take the water depth to be 17 m, and use a coastline normal of 265°T. The offshore direction of each of the two wave systems observed in Figure 14 is taken to be the direction of the higher frequency waves. Equation 6.1 is then employed to determine the local wave direction at lower frequencies. The result, shown in Figure 15, is seen to be in reasonable agreement with the data. From the figure it appears that the waves are independent of the bathymetry for wave frequencies above roughly $0.25\sqrt{g/H} \sim 0.2$ Hz.

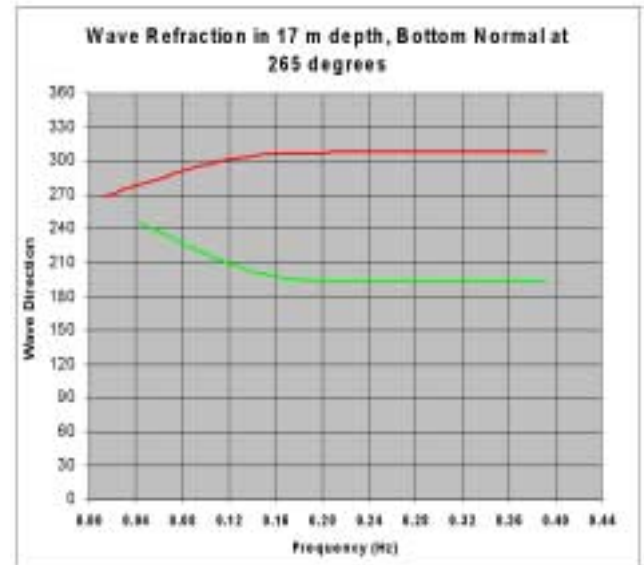


Figure 15. Modeled refraction computed using Snell’s law for the wave systems shown in Figure 14.

7. Dispersive Propagation

Because gravity waves in all but the shallowest waters are dispersive, waves generated by a distant storm will arrive in a temporal succession that is determined by their group velocity (and hence frequency), with the lower frequencies preceding the higher. This phenomenon was pointed out, and thoroughly studied, in the pioneering work of Munk *et al.* (1963), and Snodgrass *et al.* (1966). The latter investigators set up a series of observing stations across the Pacific from New Zealand to Alaska, and were able to track swell generated in the Southern Ocean as it propagated northward along a great circle into the Gulf of Alaska.

Following the development in Munk *et al.* (1963), the propagation time T for a wave of frequency f to travel a distance R is

$$T(f) = R/C_g = (4\pi R/g)f \quad (7.1)$$

where we have used the deep water form of the group velocity C_g . The travel time for waves to arrive is given by $T(f=0)$. Alternatively viewing (7.1) as a relationship for $f(T)$, we define the slope $S = df/dT$. Then the range to the generation region is given by

$$R = g/(4\pi S) = (67.4 \text{ km-Hz/day})/S \quad (7.2)$$

In this section we identify the dispersive propagation of waves generated (we hypothesize) by a distant storm. The data we examine are the group of arrivals marked as ‘‘A’’ on Figure 5. Various frequency components arrive over roughly a 4-5 day interval from 24-28 September, 1999 (spanning bursts 63-89). A plot of the peak frequency of the non-directional spectrum as a function of time (measured every four hours) is shown in Figure 16. A least squares fit to the data gives a slope S of 1 Hz per 119 days. This gives a range of roughly 8800 km, and a propagation time of 9 days for the lowest frequency waves, which first arrived at 1300Z on 24 September. Taking a deep-water direction of $281^\circ T$, we use spherical geometry to estimate that the storm was located slightly west of Guam around $13^\circ N, 140^\circ E$.

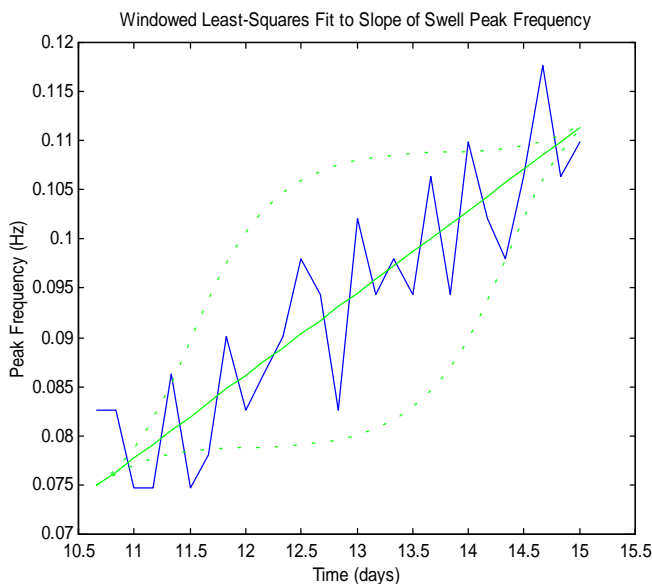


Fig. 16. Least-squares fit to slope of ridge, using the peak frequency of the non-directional spectrum measured every four hours. A cosine-squared weighting window (indicated with dashed lines) was applied to make the estimate insensitive to the choice of endpoints. Day 10.5 is 9/24/99, and the first data point shown corresponds to burst 63 in Figure 5.

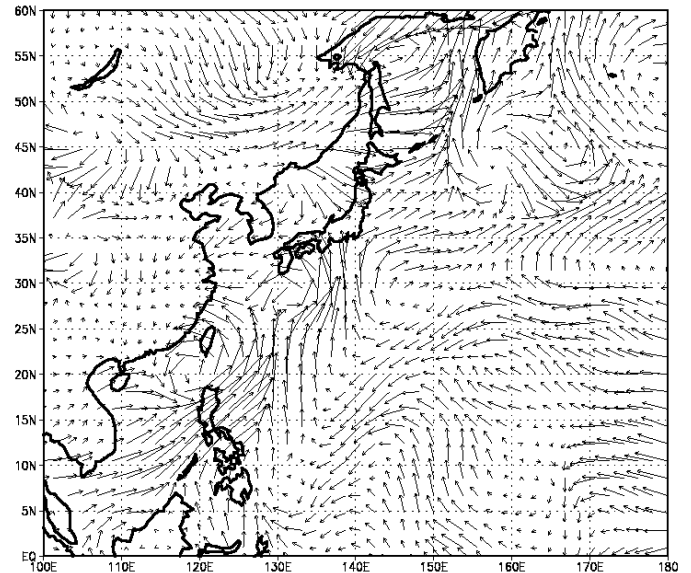


Figure 17. 12-hour average 10 m wind vectors for 1200Z September 13 taken from the 1999 NCEP/NCAR Reanalysis CD-ROM (Kalnay *et al.*, 1996). A moderate wind event can be seen in the eastern Pacific around $15^\circ N, 125^\circ E$. This figure was produced using the GrADS visualization package v1.4 (Doty, 1994).

We used the NCEP/NCAR reanalysis output (Kalnay, 1996) to look for a possible generation event. There was a moderate cyclonic disturbance with 20-30 kt winds in the vicinity of the Phillipines lasting from September 11-14. This is somewhat earlier and farther west than our earlier estimate of the source location. However, Snodgrass *et al.* (1966) noted that arrivals typically build up in amplitude over several days before reaching a plateau. Therefore this weather pattern might still be consistent with the data shown in Figure 5, although a detailed analysis of the time dependence of amplitude, which we have not carried out, would be required to determine this. Lastly, we note that the NCEP/NCAR output indicates several intense storms in the eastern Pacific during the period 15-23 September. The effect of these wind fields on the propagation of the waves is unknown, and adds a considerable degree of ambiguity to our conclusions as to their origin.

We close by noting that another example of dispersive propagation is provided by the very long waves seen at the start of the data shown in Figure 5 (spanning bursts 4-24). The shallower slope of the $f(T)$ curve in that case suggests waves arriving from the southern hemisphere. The frequency changes from .050 Hz to .075 Hz over a period of 108 hours, and a range calculation places the storm at a distance of about 13000 ± 1000 km. Waves in this frequency range will experience substantial refraction due to the bottom. Applying a refraction model to the observed direction of $240^\circ T$ (and assuming a coast normal of $260^\circ T$), gives a deep water direction of about $190^\circ T$.

8. Conclusions

We have used observations of waves and currents obtained with an ADCP to illustrate several aspects of wave-current interaction. Our measurements show that the kinematic effect of the change in wavelength of waves riding on currents must be accounted for in order to obtain the correct wave height spectrum from subsurface pressure or velocity measurements. In addition, there is a dynamical effect whereby the waves are changed in amplitude through their interaction with the current. We have shown that in a tidally-driven current regime the observed modulation of wave amplitude at the dominant tidal frequency can largely be explained by this mechanism. We have also shown that because of its directional resolution, an ADCP wave gage is a useful tool for studying refractive effects. Lastly we have revisited the dispersive arrival of waves from a distant storm.

Acknowledgments

We thank Drs. K.R. Stapleton and S. Redford of Emu Environmental Ltd. for permission to include Figure 1. N.C. Kraus acknowledges permission by Headquarters, U.S. Army Corps of Engineers, to publish this information supported by the Coastal Inlets Research Program. E. Terray was partially supported by NSF grant OCE-9811316, and ONR grant N00014-97-10483. This is WHOI contribution number 10326.

References

- Battjes (1982): A case study of wave height variations due to currents in a tidal entrance. *Coastal Engr.*, **6**, 47-57.
- Doty, Brian (1994): GrADS (Grid Analysis and Display System), v.1.4. Center for Ocean-Land-Atmosphere Interactions, Institute of Global Environment and Society, 4041 Powder Mill Rd., Suite 302, Calverton, MD 20705-3106. <http://grads.iges.org/> (192.239.84.50).
- Kalnay, E., M. Kanamitsu, R. Kistler, W. Collins, D. Deaven, L. Gandin, M. Iredell, S. Saha, G. White, J. Woollen, Y. Zhu, A. Leetmaa, R. Reynolds, M. Chelliah, W. Ebisuzaki, W. Higgins, J. Janowiak, K. C. Mo, C. Ropelewski, J. Wang, Roy Jenne, and Dennis Joseph, (1996): The NCEP/NCAR 40-Year Reanalysis Project. *Bull. Am. Met. Soc.*, **77**(3), 437-471. NCEP/NCAR Reanalysis CD-ROM: 1999.
- Gonzalez, F.I. (1984): A case study of wave-current-bathymetry interactions at the Columbia River entrance. *J. Phys. Oceanogr.*, **14**, 1065-1078.
- Gordon, R.L., E. Terray and B. Brumley (1998): Observing wave height and direction with conventional (Janus-style) ADCPs. *Proc. Oceanology International'98*, **2**, 261-269, ISBN 0 900254 21 1.
- Hashimoto, N. (1997): Analysis of the directional wave spectrum from field data. *Advances in Coastal and Ocean Engineering.*, vol. **3**, pp. 103-143. World Science Press.
- Kirby, J.T. and T-M. Chen (1989): Surface waves on vertically sheared flows: approximate dispersion relations. *J. Geophys. Res.*, **94**(C1), 1013-1027.
- Krogstad, H.E., R.L. Gordon and M.C. Miller (1988): High-resolution directional wave spectra from horizontally-mounted acoustic Doppler current meters. *J. Atmos. and Oceanic Technol.*, **5**, 340-352.
- Munk, W.H., G.R. Miller, F.E. Snodgrass and N.F. Barber (1963): Directional recording of swell from distant storms. *Proc. Roy. Soc.* **A255**, 505-584.
- Snodgrass, F.E., G.W. Groves, K.F. Hasselmann, G.R. Miller, W.H. Munk and W.H. Powers (1966): Propagation of ocean swell across the Pacific. *Proc. Roy. Soc.* **A259**, 431-497.
- Strong, B., B. Brumley, E.A. Terray, and G.W. Stone (2000): The performance of ADCP-derived wave directional spectra and comparison with other independent measurements. *Proc. Oceans2000*, IEEE Press, 1195-1203.
- Terray, E.A., B.H. Brumley and B. Strong (1999): Measuring waves and currents with an upward-looking ADCP. *Proc. IEEE 6th Working Conference on Current Measurement*, IEEE Press, 66-71.
- Terray, E.A., R.L. Gordon and B.H. Brumley (1997): Measuring wave height and direction using upward-looking ADCPs. *Proc. Oceans'97*, IEEE Press, 287-290.
- Terray, E.A., H.E. Krogstad, R. Cabrera, R.L. Gordon and A. Lohrmann (1990): Measuring wave direction using upward-looking Doppler sonar. *Proc. IEEE 4th Working Conference on Current Measurement*, IEEE Press, 252-257
- Thomas, G.P. (1981): Wave-current interactions: An experimental and numerical study. Part 1. Linear Waves. *J. Fluid Mech.*, **110**, 457-474.